Bearing Fault Detection in Induction Motors Using Line Currents

Sunder Muthukumaran[1], **Abishek Rammohan**[1], **Sabarivelan Sekar**[1], **Monalisa Maiti**[1], and **Kishore Bingi**[2†], Non-members

ABSTRACT

This paper focuses on the development of a bearing fault detection model for induction motors using line currents. The graphical and numerical analysis of the model is conducted using Park's vector approach and envelope signals based on the Hilbert transform. The proposed model is evaluated on currents measured using eight different types of induction motors. The graphical results from the Concordia pattern between d and q-components of stator currents show that healthy bearing behavior is circular compared to that of the elliptical faulty bearing. The numerical results demonstrate that the minimum and maximum envelopes for the d and q-components of the stator currents are significant at more than one. The sum of kurtosis for the envelope signal of d and q-components in the stator currents is more significant at less than 5.0.

Keywords: Bearing, Concordia Pattern, Envelope, Hilbert Transform, Induction Motor, Park's Vector

1. INTRODUCTION

Induction motors are mainly used in residential and industrial applications such as transportation, mining, chemicals, power plants, and paper for electrical to mechanical energy conversion [1] due to their high reliability, robustness, and cost-effectiveness. However, the main issue with the operation of induction motors is that such harsh industrial application has affected their reliability, causing unexpected breakdowns, resulting in high maintenance costs and motor deterioration [2, 3]. Scheduled maintenance and replacement are the primary methods for improving the reliability of these motors. During scheduled maintenance, the
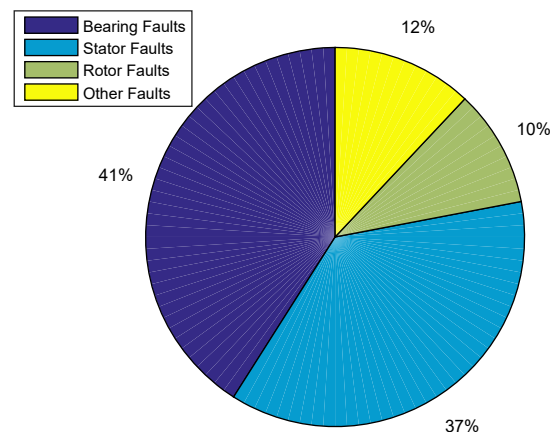
Fig. 1: *Survey analysis from electric power research institute [10].*

motor is examined regularly, while parts of the motor are replaced periodically during scheduled replacement. Planned replacement is simple but very expensive compared to planned maintenance [4]. Condition-based monitoring determines the condition of the induction motor based on the data collected using external sensors. This method involves continuous monitoring of the induction motor together with periodical motor maintenance [5]. Generally, condition-based monitoring is performed through visual inspection or a fault diagnosis system which monitors the vibrations, over-currents, and high temperatures of the motor to detect faults. The two types of condition-based monitoring techniques are online and offline tests [6]. The online tests are performed without isolating the motor from the power supply, while the offline test is performed by isolating the motor from the power supply [7].

Induction motors are often exposed to harsh environments such as overloading, unsafe operation, insufficient cooling, and lack of lubrication. The main factors affecting the failure of induction motors in these extreme environments are unstable power supply, thermal overload, high-speed oscillation, short-circuiting in the stator winding, broken rotor bars, and gear and ball bearing failure [8, 9]. As shown in Fig. 1, 41% of induction motor failures are due to a fault in the bearing, 37% stator faults, 10% rotor, and 12% other faults [10]. Thus, the overall defects in motors can be classified as follows:

Fig. 2: *Ball bearing structure.*

- Electrical defects
  - Stator winding faults
  - Rotor faults
- Mechanical defects
  - Bearing faults
  - Dynamic, static,t and mixed eccentricities
  - Gear faults

The continuous replacement and preventive maintenance of bearings are essential factors in the smooth operation of induction motors [11, 12]. The bearings in the motor are connected to the rotor, which is used to minimize friction between the shafts and stationary parts. Bearing faults are mainly due to lubricant-related failures, which can be avoided by early prediction and preventive maintenance [13]. The ball bearing structure shown in Fig. 2 consists of several balls placed in between the inner and outer races. A cage is used to maintain a uniform distance between the balls. During regular operation, several stresses are likely to develop in the induction motor, causing fatigue in the inner and outer races. This leads to localized defects, causing holes, dents, and pitting in the outer race, and the distributed defects create surface roughness in the inner race of the bearings.

Over the years, researchers have proposed several invasive, and non-invasive techniques [4] as follows [14, 15]:

- Invasive analysis [16]
  - Acoustic emission analysis
  - Thermal analysis
  - Sound analysis
  - Chemical analysis
  - Vibration analysis
- Non-invasive analysis
  - Motor current pattern analysis
  - Wavelet analysis
  - Park's vector analysis
  - Power analysis

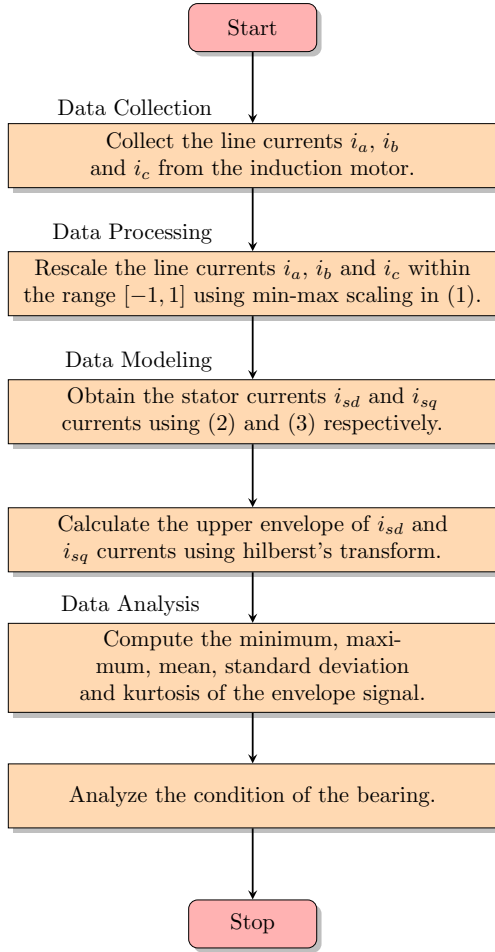Invasive techniques are difficult to implement and

very expensive compared to non-invasive. This is because various sensors need to be installed to measure acoustic, thermal, sound, and vibration signals [16]. Thus, it is not easy to install sensors and high installation and maintenance costs are involved. On the other hand, among the non-invasive techniques, the power analysis and Park vector approaches are more suitable for bearing fault detection and diagnosis [4, 15, 17].

Several researchers have used power analysis for the detection of rotor bars and eccentricity faults. However, it has been concluded that such investigation is not practical during no-load operation of the induction motor [18]. Park's vector analysis has been mainly used to detect localized faults in the bearings, rotor, and stator. In this analysis, the three-phase AC currents i_a, i_b, and i_c are transformed to d and q-components with currents of i_d and i_q to eliminate the time-varying effects of inductance [17, 19]. Under ideal conditions, the pattern between i_d and i_q will be circular. However, in the case of faults or damaged bearings, the pattern is no longer circular and forms various patterns. Thus, based on a different pattern, the type of fault inside the induction motor can be analyzed. The thickness of the pattern also provides information on the harmonics induced due to localized defects in the bearings of the induction motor.

The reseachers in [20] and [21] used Park's vector analysis to detect stator faults in induction motors under varying loads. The authors of [22] used Park's vector analysis to detect the faults in the outer race of the bearing. Furthermore, they also proposed an analysis method for measuring the thickness of the pattern. Similarly, the detection of dynamic, static, and mixed eccentricity faults has also been achieved using Park's vector analysis in [23], [24], and [25]. Furthermore, stator inter-turn faults for surface-mounted permanent magnet synchronous motors have also been detected using Park's vector analysis [19]. On the other hand, for the classification of various faults, a neural network-based approach has been proposed in [26].

In the overall comparison, both Park's vector and power analysis techniques are revealed to be inexpensive. The Park's vector approach can detect bearing faults, while power analysis can detect faults in rotor bars and eccentricity. However, further investigation is needed to determine a suitable analysis method for bearing-distributed faults. In power analysis, fault detection is affected by external noise, and the capability to analyze mechanical faults requires verification.

With this motivation, a graphical analysis for bearing fault detection in induction motors using line currents based on Park's vector approach and the Concordia pattern is proposed in this paper. Furthermore, numerical analysis for envelope signals

Fig. 3: *Flowchart of proposed methodology.*

Fig. 4: *Experimental setup for data collection.*

Fig. 5: *Concordia pattern between i_{sd} and i_{sq} for a healthy motor.*

using Hilbert's transform is proposed for bearing fault detection.

The paper's remaining sections are organized as follows: Section 2 presents the proposed methodology. The results and a discussion on the methodology are presented in Section 3, while Section 4 concludes the paper.
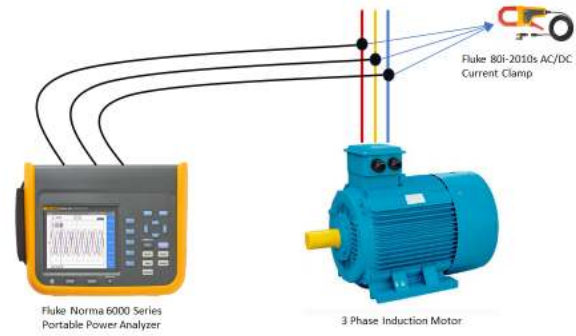
2. PROPOSED METHODOLOGY

A flowchart of the proposed methodology is presented in Fig. 3, consisting of four stages: data collection, processing, modeling, and analysis, all of which are elaborated in the following subsections.
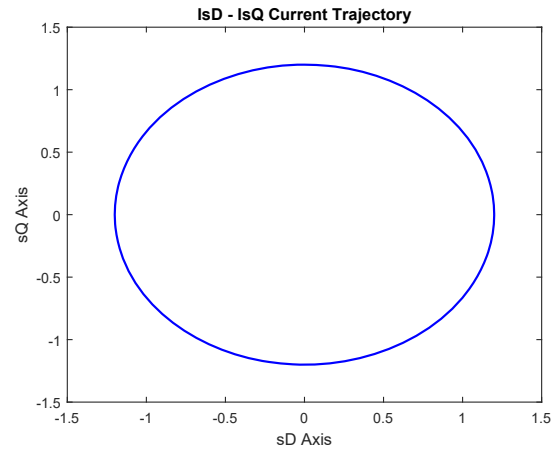
2.1 Data Collection and Processing

The line currents i_a, i_b, and i_c from the three-phase induction motor are collected using the Fluke Norma 6000 series portable power analyzer shown in Fig. 4. The measurements are performed using Fluke 80i-2010s AC/DC clamp with $2000\,\mathrm{A}$ range. The collected data by the meter is exported to the PC using Fluke power analyzer software for data processing.

For consistent analysis of the different motor ranges, the line currents i_a, i_b, and i_c are normalized to the range of $[-1, 1]$ using min-max scaling, defined as follows [27]:

$$Y = \frac{2(X - X_{\min})}{X_{\max} - X_{\min}} - 1 \qquad (1)$$

where $X_{\min}$ and $X_{\max}$ are the minimum and maximum value of X, respectively.

2.2 Data Modeling and Analysis

The d and q-components of the stator currents are obtained from the normalized i_a, i_b, and i_c using Park's vector transform [17],

$$i_{sd} = \sqrt{\frac{2}{3}}i_a - \sqrt{\frac{1}{6}}i_b - \sqrt{\frac{1}{6}}i_c \qquad (2)$$

$$i_{sq} = \sqrt{\frac{1}{2}}i_b - \sqrt{\frac{1}{2}}i_c \qquad (3)$$

where i_a, i_b, and i_c are three-phase AC currents, i_{sd} and i_{sq} are d and q-component currents.

From Eqs. (2) and (3), for a healthy motor bearing, the Concordia pattern between i_{sd} and i_{sq} is a uniform circle, with the center of origin as indicated in Fig. 5. In the case of a faulty or damaged

Original Signal
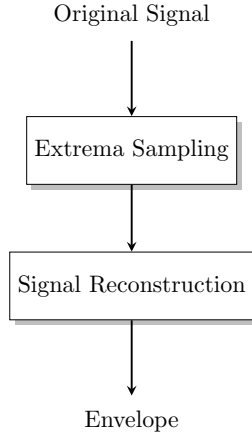
Fig. 6: *Envelope calculation process.*

bearing, the pattern is no longer circular and becomes elliptical. Furthermore, it should be noted that in ideal conditions, only fundamental harmonics exist in the motor. In non-ideal conditions, the motor contains odd harmonics, induced due to symmetry in the motor structure and power supply.

Thus, under ideal conditions, the d and q-components are simplified as,

$$i_{sd} = \frac{\sqrt{6}}{2} I_m \sin(\omega t) \tag{4}$$

$$i_{sq} = \frac{\sqrt{6}}{2} I_m \sin\left(\omega t - \frac{\pi}{2}\right) \tag{5}$$

where I_m is the maximum value of the supply phase current, ω is the angular frequency, and t is the time.

To further analyze the condition of the bearing, the upper envelope signals of i_{sd} and i_{sq} are calculated using Hilbert's transform. For a given modulated signal $g(t)$ and its Fourier transform $S(f)$, the Hilbert transform is given as follows [28]:

$$\begin{aligned} \tilde{g}(t) &= H[g(t)] \\ &= p\frac{1}{\pi} \int_{-\infty}^{\infty} \frac{g(\tau)}{t - \tau} d\tau \end{aligned} \tag{6}$$

where p is the Cauchy principal value. The analytic signal $\mathcal{N}(g(t))$ is given as,

$$\mathcal{N}(g(t)) = g(t) + j\tilde{g}(t) \tag{7}$$

From Eq. (7), the envelope of modulated signal $g(t)$ can be obtained as,

$$|\mathcal{N}(g(t))| = \sqrt{g^2(t) + \tilde{g}^2(t)} \tag{8}$$

From Eq. (8), the upper and lower envelopes of the original signal can be obtained in two stages, as shown in Fig. 6. Firstly, the local minima and maxima is obtained for the lower and upper envelopes, respectively. The signal between the local

Table 1: *Motor Specifications.*

Motor ID	Power (kW)	Speed (rpm)
EM1 #100	75	3000
EM1 #200	30	3000
EM1 #300	30	1000
EM1 #400	30	1000
EM1 #500	30	1000
EM1 #600	25	1000
EM1 #700	25	1000
EM1 #800	15	1000

minima or maxima for the lower or upper envelopes then reconstructed using a cubic spline.

For the numerical analysis, the statistics are computed for the upper envelope of i_{sd} and i_{sq} from Eq. (8) in terms of mean, standard deviation, and kurtosis as follows [29]:

$$\overline{Y} = \frac{1}{n} \sum_{i=1}^{n} Y_i \tag{9}$$

$$\sigma = \sqrt{\frac{\sum_{i=1}^{n}(Y_i - \overline{Y})^2}{n}} \tag{10}$$

$$K = n \times \frac{\sum_{i=1}^{n}(Y_i - \overline{Y})^4}{\sum_{i=1}^{n}(Y_i - \overline{Y}^2)^2} \tag{11}$$

where n is the number of samples, $\overline{Y}$ is the mean, σ is the standard deviation, and K is the kurtosis.

3. RESULTS AND DISCUSSION

This section presents the measurement of line currents from eight different induction motors normalized using min-max scaling. The modeling and numerical results are obtained using Park's vector analysis and envelope signals, respectively.

3.1 Data Collection and Processing

In this analysis, the line currents are measured using eight different three-phase induction motors as per the experimental setup in Fig. 4. The specifications for the motors are presented in Table 1. The line currents of these eight induction motors are shown in Figs. 7(a)–7(h). Figs. 7(a) and 7(b) show that the line currents of motors EM1 #100 and EM1 #200 range from −200 to 200 A and −100 to 100 A, respectively. In Figs. 7(c), 7(d), and 7(e), the line currents of motors EM1 #300, EM1 #400, and EM1 #500 range from −50 to 50 A. Figs. 7(f) and 7(g) show that the line currents of motors EM1 #600 and EM1 #700 range from −30 to 30 A. Fig. 7(h)

(a) EM1 #100

(b) EM1 #200

(c) EM1 #300

(d) EM1 #400

(e) EM1 #500

(f) EM1 #600

(g) EM1 #700
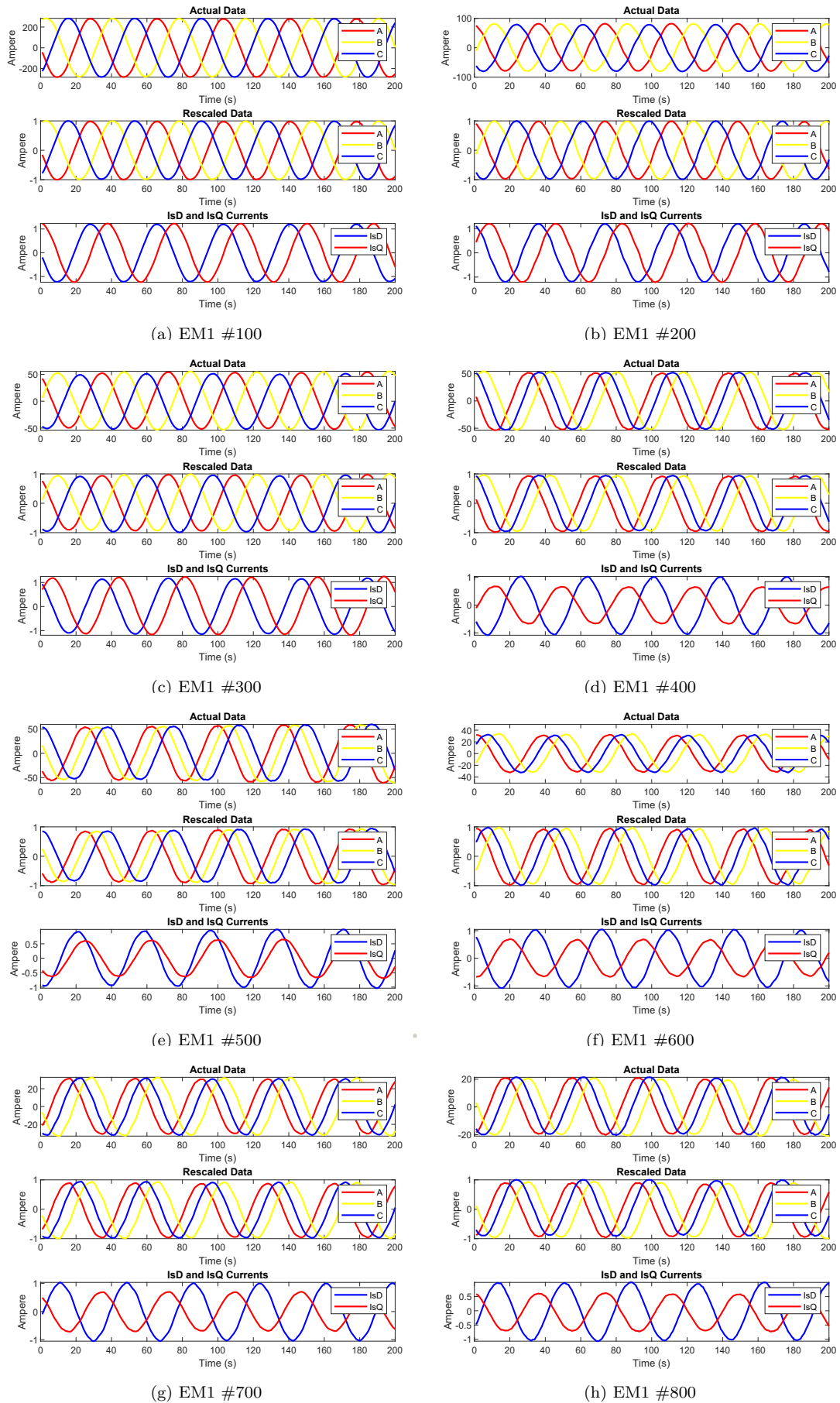
(h) EM1 #800

Fig. 7: *Actual, rescale, and stator currents of the induction motors.*

(a) EM1 #100

(b) EM1 #200

(c) EM1 #300

(d) EM1 #400

(e) EM1 #500

(f) EM1 #600

(g) EM1 #700
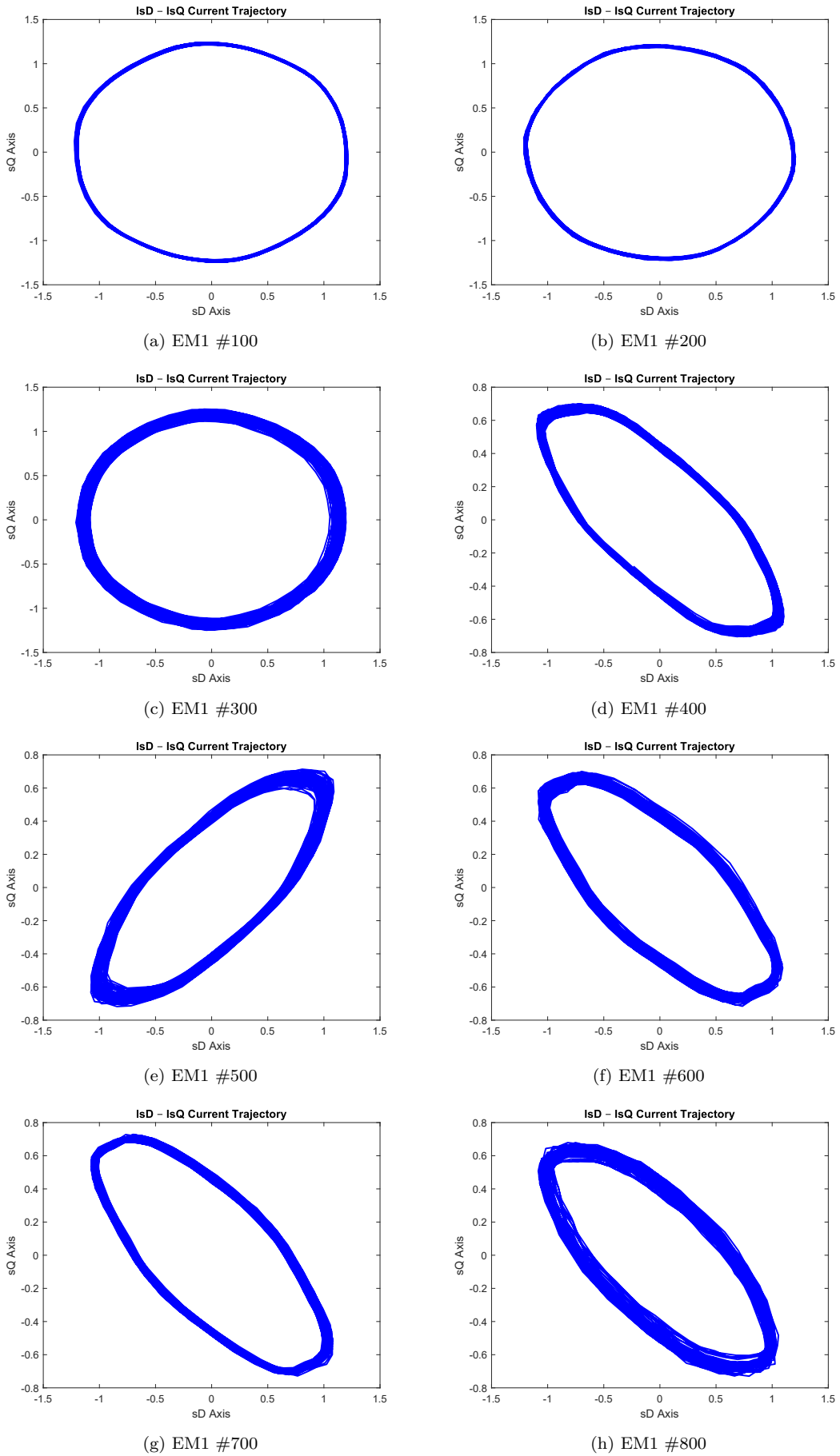
(h) EM1 #800

Fig. 8: *Concordia pattern between i_{sd} and i_{sq} of the induction motor.*

shows that the line currents of motor EM1 #800 range from -20 to $20\,\mathrm{A}$.

For consistent analysis of all eight motors in these different ranges, the line currents i_a, i_b, and i_c are normalized to $[-1, 1]$ using min-max scaling as defined in Eq. (1). The rescaled line currents of all eight induction motors in the range $[-1, 1]$ are shown in Figs. 7(a)–7(h).

3.2 Data Modeling and Analysis

The d and q-components of the stator currents can be obtained from the normalized i_a, i_b, and i_c using Park's vector transform as defined in Eqs. (2) and (3). Thus, the stator currents isd and isq of all eight induction motors are also shown in Figs. 7(a)–7(h). It can be observed from Figs. 7(a)–7(c) that the i_{sd} and i_{sq} currents of motors EM1 #100, EM1 #200, and EM1 #300 range from -1.2 to $1.2\,\mathrm{A}$ approximately. In Figs. 7(d)–7(h), the i_{sd} and i_{sq} currents of motors EM1 #400, EM1 #500, EM1 #600, EM1 #700, and EM1 #800 range from about -1.2 to $1.2\,\mathrm{A}$ and -0.7 to $0.7\,\mathrm{A}$, respectively.

The Concordia pattern between i_{sd} and i_{sq} for all eight induction motors is shown in Figs. 8(a)–8(h). It can be observed from Figs. 8(a)–8(c) that the Concordia pattern of motors EM1 #100, EM1 #200, and EM1 #300 are circular. Thus, it can be concluded that the bearings of motors EM1 #100, EM1 #200, and EM1 #300 are healthy. In Figs. 8(d)–8(h), the Concordia pattern between i_{sd} and i_{sq} is elliptical. Thus, it can be concluded that the bearings of motors EM1 #400, EM1 #500, EM1 #600, EM1 #700, and EM1 #800 are faulty. The fault is either in the outer or inner race, cage, or ball. Furthermore, the pattern also confirms a severe fault in the short circuit winding of the induction motor.

The upper envelope signal of i_{sd} and i_{sq} using Eq. (8) is calculated to strengthen the analysis further. Thus, the envelope signals of i_{sd} and i_{sq} for all eight induction motors are shown in Figs. 9(a)–9(h). It can be observed from Figs. 9(a)–9(c) that the envelope of i_{sd} and i_{sq} currents of motors EM1 #100, EM1 #200, and EM1 #300 range from approximately 1.0 to $1.25\,\mathrm{A}$. In Figs. 9(d)–9(h), the i_{sd} and i_{sq} currents of motors EM1 #400, EM1 #500, EM1 #600, EM1 #700, and EM1 #800 range from approximately 0.9 to $1.1\,\mathrm{A}$ and 0.55 to $0.75\,\mathrm{A}$, respectively.

The envelope signal statistics i_{sd} and i_{sq} for all eight induction motors in terms of minimum, maximum, mean, standard deviation, and kurtosis as defined in Eqs. (9), (10), and (11) are shown in Table 2 and Fig. 10. Minimum values greater than one for both i_{sd} and i_{sq} denotes a healthy result. Thus, the minimum values of i_{sd} and i_{sq} for motors EM1 #100, EM1 #200, and EM1 #300 are greater than those denoting healthy bearings.

For the remaining motors EM1 #400, EM1 #500, EM1 #600, EM1 #700, and EM1 #800, the minimum value of both i_{sd} and i_{sq} is less than one, which denotes faulty bearings. Similarly, from the maximum values, it can be concluded that values greater than one for both i_{sd} and i_{sq} denotes healthy bearings. Thus, the maximum values of i_{sd} and i_{sq} for motors EM1 #100, EM1 #200, and EM1 #300 are significant at more than one and denote a healthy bearing. For the remaining motors EM1 #400, EM1 #500, EM1 #600, EM1 #700, and EM1 #800, the maximum value of i_{sd} and i_{sq} is significant at more than one and less than one, respectively, denoting a faulty bearing.

From the kurtosis values, which are a combination of the mean and standard deviation defined in Eq. (11), it can be concluded that the sum of kurtosis i_{sd} and i_{sq} is less than 5.0, denoting healthy bearings. For motor EM1 #300, the sum of kurtosis is less than 5.0, which indicates a healthy bearing. For the remaining motors EM1 #100, EM1 #200, EM1 #400, EM1 #500, EM1 #600, EM1 #700, and EM1 #800, the sum of kurtosis is significant at more than 5.0, denoting faulty bearings.

Therefore, from the graphical analysis, it can be concluded that a circular Concordia pattern between i_{sd} and i_{sq} denotes a healthy bearing. In addition, from the numerical analysis, the minimum and maximum values i_{sd} and i_{sq} are significant at more than one, while the sum of kurtosis isd and isq is significant at less than 5.0.

4. CONCLUSION

In this paper, a bearing fault detection model is developed for induction motors using line currents. The graphical analysis of the model uses Park's vector approach. The Concordia pattern obtained between i_{sd} and i_{sq} using Park's vector approach indicates that a healthy bearing is circular compared to the elliptical behavior of a faulty motor. The numerical analysis of the model is based on envelope signal components of i_{sd} and i_{sq}. The proposed approach is evaluated on currents measured from eight different types of induction motors. From the numerical analysis, it can be concluded that the minimum and maximum envelopes of i_{sd} and i_{sq} are significant at more than one, while the sum of kurtosis i_{sd} and i_{sq} is significant at less than 5.0. Therefore, based on this graphical and numerical analysis, it can be observed that the EM1 #300 bearing is healthy, and the remaining motors have a faulty bearing.

In future work, the harmonics induced in the induction motor will be analyzed based on pattern thickness. Furthermore, bearing faults will be classified using neural networks.
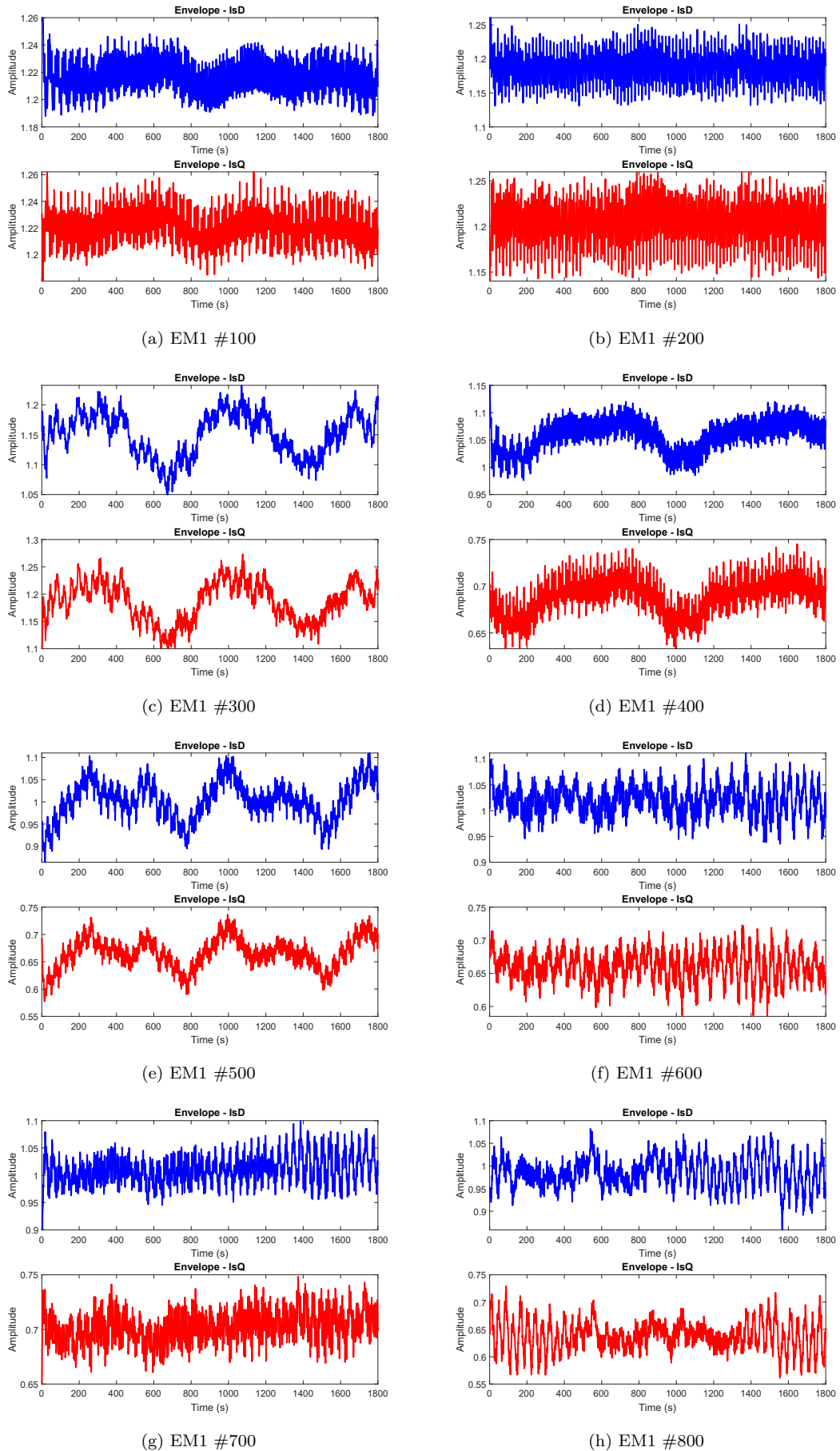
Fig. 9: *Envelope signals of i_{sd} and i_{sq} currents in induction motors.*

Table 2: *Statistics for envelope signals of i_{sd} and i_{sq}.*

Motor ID	Envelope of i_{sd}					Envelope of i_{sq}				
	Min	Max	Mean	Std Dev	Kurtosis	Min	Max	Mean	Std Dev	Kurtosis
EM1 #100	1.1802	1.3414	1.2122	0.0142	10.4301	1.1843	1.2649	1.2240	0.0134	2.6604
EM1 #200	1.1310	1.2605	1.1898	0.0237	2.5469	1.0676	1.2618	1.2038	0.0244	3.0350
EM1 #300	1.0500	1.2326	1.1520	0.0360	2.2468	1.0055	1.2731	1.1868	0.0358	2.5619
EM1 #400	0.9651	1.2420	1.0511	0.0298	3.6181	0.6262	0.7452	0.6892	0.0208	2.6558
EM1 #500	0.8620	1.1095	1.0050	0.0425	2.8570	0.5784	0.7349	0.6671	0.0275	2.9452
EM1 #600	0.9093	1.1117	1.0198	0.0294	2.9239	0.5850	0.7228	0.6608	0.0227	2.8393
EM1 #700	0.6847	1.1077	1.0115	0.0302	17.566	0.5628	0.7483	0.7033	0.0156	6.0159
EM1 #800	0.8283	1.0800	0.9652	0.0345	3.1237	0.5735	0.7422	0.6579	0.0287	2.9296
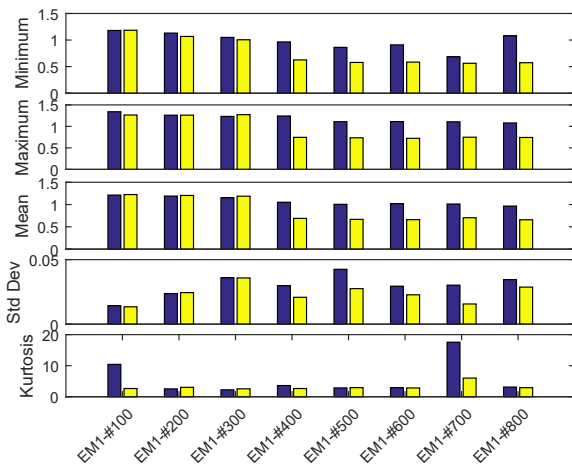
Fig. 10: *Analysis of envelope signals i_{sd} and i_{sq}.*

REFERENCES

[1] O. AlShorman, M. Irfan, N. Saad, D. Zhen, N. Haider, A. Glowacz, and A. AlShorman, "A review of artificial intelligence methods for condition monitoring and fault diagnosis of rolling element bearings for induction motor," *Shock and Vibration*, vol. 2020, 2020, Art. no. 8843759.

[2] Y. Kumsuwan, W. Srirattanawichaikul, and S. Premrudeepreechacharn, "Reduction of torque ripple in direct torque control for induction motor drives using decoupled amplitude and angle of stator flux control," *ECTI Transactions on Electrical Engineering, Electronics, and Communications*, vol. 8, no. 2, pp. 187–196, 2010.

[3] Z. Y. M. Hurtado, C. P. Tello, and J. G. Sarduy, "A review on detection and fault diagnosis in induction machines," *Publicaciones en Ciencias y Tecnología*, vol. 8, no. 1, pp. 11–30, 2014.

[4] M. Irfan, N. Saad, R. Ibrahim, V. S. Asirvadam, A. Alwadie, and M. A. Sheikh, "An assessment on the non-invasive methods for condition monitoring of induction motors," in *Fault Diagnosis and Detection*, M. Demetgul and M. Ünal, Eds., London,

UK: IntechOpen, 2017. [Online]. Available: https://www.intechopen.com/books/fault-diagnosis-and-detection/an-assessment-on-the-non-invasive-methods-for-condition-monitoring-of-induction-motors

[5] A. Choudhary, D. Goyal, S. L. Shimi, and A. Akula, "Condition monitoring and fault diagnosis of induction motors: A review," *Archives of Computational Methods in Engineering*, vol. 26, no. 4, pp. 1221–1238, 2019.

[6] A. Gandhi, T. Corrigan, and L. Parsa, "Recent advances in modeling and online detection of stator interturn faults in electrical motors," *IEEE Transactions on Industrial Electronics*, vol. 58, no. 5, pp. 1564–1575, 2010.

[7] M. Geethanjali and H. Ramadoss, "Fault diagnosis of induction motors using motor current signature analysis: A review," in *Advanced Condition Monitoring and Fault Diagnosis of Electric Machines*, M. Irfan, Ed., IGI Global, 2019, pp. 1–37.

[8] Y. Liu and A. M. Bazzi, "A review and comparison of fault detection and diagnosis methods for squirrel-cage induction motors: State of the art," *ISA Transactions*, vol. 70, pp. 400–409, 2017.

[9] A. Heng, S. Zhang, A. C. Tan, and J. Mathew, "Rotating machinery prognostics: State of the art, challenges and opportunities," *Mechanical systems and signal processing*, vol. 23, no. 3, pp. 724–739, 2009.

[10] K. D. Kompella, M. V. G. Rao, and R. S. Rao, "Bearing fault detection in a 3 phase induction motor using stator current frequency spectral subtraction with various wavelet decomposition techniques," *Ain Shams Engineering Journal*, vol. 9, no. 4, pp. 2427–2439, 2018.

[11] Y. Wei, Y. Li, M. Xu, and W. Huang, "A review of early fault diagnosis approaches and their applications in rotating machinery," *Entropy*, vol. 21, no. 4, 2019, Art. no. 409.

[12] P. Zhang, Y. Du, T. G. Habetler, and B. Lu, "A survey of condition monitoring and protection methods for medium-voltage induction motors,"

IEEE Transactions on Industry Applications, vol. 47, no. 1, pp. 34–46, 2010.

[13] A. Boudiaf, A. Djebala, H. Bendjma, A. Balaska, and A. Dahane, "A summary of vibration analysis techniques for fault detection and diagnosis in bearing," in *2016 8th International Conference on Modelling, Identification and Control (ICMIC)*, 2016, pp. 37–42.

[14] H.-Q. Wang, W. Hou, G. Tang, H.-F. Yuan, Q.-L. Zhao, and X. Cao, "Fault detection enhancement in rolling element bearings via peak-based multiscale decomposition and envelope demodulation," *Mathematical Problems in Engineering*, vol. 2014, 2014, Art. no. 329458.

[15] A. Alwadie, "The decision making system for condition monitoring of induction motors based on vector control model," *Machines*, vol. 5, no. 4, 2017, Art. no. 27.

[16] Z. Gao, C. Cecati, and S. X. Ding, "A survey of fault diagnosis and fault-tolerant techniques—part i: Fault diagnosis with model-based and signal-based approaches," *IEEE Transactions on Industrial Electronics*, vol. 62, no. 6, pp. 3757–3767, 2015.

[17] J. Zarei and J. Poshtan, "An advanced park's vectors approach for bearing fault detection," *Tribology International*, vol. 42, no. 2, pp. 213–219, 2009.

[18] I. Ahmed, "Investigation of single and multiple faults under varying load conditions using multiple sensor types to improve condition monitoring of induction machines" Ph.D. dissertation, School of Electrical and Electronic Engineering, University of Adelaide, Australia, 2008.

[19] S. S. Kuruppu and N. A. Kulatunga, "DQ current signature-based faulted phase localization for SM-PMAC machine drives," *IEEE Transactions on Industrial Electronics*, vol. 62, no. 1, pp. 113–121, 2014.

[20] D. V. Spyropoulos and E. D. Mitronikas, "Induction motor stator fault diagnosis technique using park vector approach and complex wavelets," in *2012 20th International Conference on Electrical Machines*, 2012, pp. 1730–1734.

[21] A. P. Parra, M. C. A. Enciso, J. O. Ochoa, and J. A. P. Peñaranda, "Stator fault diagnosis on squirrel cage induction motors by esa and epva," in *2013 Workshop on Power Electronics and Power Quality Applications (PEPQA)*, 2013, pp. 1–6.

[22] S. B. Salem, W. Touti, K. Bacha, and A. Chaari, "Induction motor mechanical fault identification using park's vector approach," in *2013 International Conference on Electrical Engineering and Software Applications*, 2013, pp. 1–6.

[23] S. B. Salem, K. Bacha, and M. Gossa, "Induction motor fault diagnosis using an improved combination of hilbert and park transforms," in *2012 16th IEEE Mediterranean Electrotechnical Conference*, 2012, pp. 1141–1146.

[24] A. Rezig, A. N'Diaye, M. Mekideche, and A. Djerdir, "Modelling and detection of bearing faults in permanent magnet synchronous motors," in *2012 20th International Conference on Electrical Machines*, 2012, pp. 1778–1782.

[25] K. Bacha, S. B. Salem, and A. Chaari, "An improved combination of hilbert and park transforms for fault detection and identification in three-phase induction motors," *International Journal of Electrical Power & Energy Systems*, vol. 43, no. 1, pp. 1006–1016, 2012.

[26] J. Zarei, "Induction motors bearing fault detection using pattern recognition techniques," *Expert Systems with Applications*, vol. 39, no. 1, pp. 68–73, 2012.

[27] A. Kallner, "Formulas," in *Laboratory Statistics: Methods in Chemistry and Health Science*, 2nd ed., Elsevier, 2018, pp. 1–140.

[28] Y. Yang, "A signal theoretic approach for envelope analysis of real-valued signals," *IEEE Access*, vol. 5, pp. 5623–5630, 2017.

[29] A. R. Bhende, G. K. Awari, and S. P. Untawale, "Comprehensive bearing condition monitoring algorithm for incipient fault detection using acoustic emission," *Jurnal Tribologi*, vol. 2, pp. 1–30, 2014.

Sunder Muthukumaran completed his higher secondary education. He is currently pursuing his Bachelor's degree (B.Tech) at the Department of Electronics and Instrumentation Engineering, School of Electrical Engineering, Vellore Institute of Technology, Vellore, India. His current research interest includes hybrid optimization algorithm. He has successfully co-prototyped All-Terrain-Rover guided by a small synchronized rotorcraft. For his passion in 3D animation and photorealistic physics simulations, he contributes to his university's animation team as an animation artist.

Abishek Rammohan graduated with flying colors and completed his higher secondary education from Maharishi Vidya Mandir Sr. Secondary School, Hosur, India. He is currently pursuing his Bachelor's degree (B.Tech) at the Department of Electronics and Instrumentation Engineering, School of Electrical Engineering, Vellore Institute of Technology, Vellore, India. His current research interest includes optimization algorithm. He is also a key contributor to the design team at his university. His interests include photography and sports, in which he has competed and won prizes in both. Being part of NCC in high school has also honed discipline and expert marksmanship skills in him.

Sabarivelan Sekar completed his higher education from Scism Matriculation Higher Secondary School, Theni, India. At present, he is doing his Bachelor's degree at the Department of Electronics and Instrumentation Engineering, School of Electrical Engineering, Vellore Institute of Technology, Vellore, India. He is also an athlete. Being an athlete, his qualities include self-confidence, self-discipline, and good time management.

Monalisa Maiti completed her higher secondary education from Air Force School Viman Nagar, Pune, India. Currently, she is pursuing her Bachelor's degree (B.Tech) in Electronics and Instrumentation Engineering at Vellore Institute of Technology, Vellore, India. Her research interests center around the development and application of a hybrid optimization algorithm. She is a part of the management department in the team Assailing Falcons and Skillship Vellore chapter. She is an aeroplane enthusiast and has a penchant for English Literature.

Kishore Bingi received his B.Tech degree in Electrical and Electronics Engineering from Bapatla Engineering College, Andhra Pradesh, India, in 2012, M.Tech degree in Instrumentation and Control Systems from National Institute of Technology (NIT) Calicut, Kerala, India, in 2014, and Ph.D. degree from the Department of Electrical and Electronic Engineering, Universiti Teknologi PETRONAS, Perak, Malaysia, in 2019. He has worked as an Assistant Systems Engineer with TATA Consultancy Service from 2014 to 2015. He has also worked as a Research Scientist and a Postdoctoral Researcher at the Institute of Autonomous Systems, Universiti Teknologi PETRONAS, from 2019 to 2020. He is currently an Assistant Professor (Senior Grade) at the Department of Control and Automation, School of Electrical Engineering, Vellore Institute of Technology, Vellore, India. His current research interests include non-linear process modeling, fractional-order control, and optimization.